N^6-adenosine methylation of mRNAs requires Wtap expression and controls T cell receptor signaling and survival

Taku Ito-Kureha
Ludwig-Maximilians-Universität, Biomedical Center (BMC) Institute for Immunology
https://orcid.org/0000-0002-6239-9227
Cristina Leoni
Institute for Research in Biomedicine
Kayla Borland
Ludwig Maximilian University of Munich
Marian Bataclan
Institute for Research in Biomedicine/ Università della Svizzera Italiana
Rebecca Metzger
Ludwig-Maximilians-Universität, Biomedical Center (BMC) Institute for Immunology
Gregor Ammann
Ludwig-Maximilians-Universität
Anne Krug
LMU Munich https://orcid.org/0000-0002-9556-7207
Annalisa Marsico
Helmholtz Center Munich
Stefanie Kellner
Ludwig-Maximilians-Universität
Stefan Canzar
Ludwig-Maximilians-Universität
Stefan Feske
New York University
Silvia Monticelli
Universita della Svizzera Italiana https://orcid.org/0000-0002-5909-8802
Julian König
7Institute of Molecular Biology
Vigo Heissmeyer (vigo.heissmeyer@med.uni-muenchen.de)
Ludwig Maximilian University of Munich https://orcid.org/0000-0002-2263-8545

Article

Keywords: T cell antigen receptor, m6A, Wtap protein

Posted Date: November 16th, 2021

DOI: https://doi.org/10.21203/rs.3.rs-1053157/v1

Version of Record: A version of this preprint was published at Nature Immunology on July 25th, 2022. See the published version at https://doi.org/10.1038/s41590-022-01268-1.

Abstract

T cell antigen receptor (TCR) signaling controls the development, activation and survival of T cells by involving several layers and numerous mechanisms of gene regulation. N6-methyladenosine (m6A) is the most prevalent mRNA modification affecting splicing, translation and stability of transcripts. Here, we describe the Wtap protein as essential for m6A methyltransferase complex function and reveal its crucial role in TCR signaling. Wtap and m6A methyltransferase functions were required for the differentiation of thymocytes, control of activation-induced death of peripheral T cells and prevention of colitis by enabling gut RORγt+ regulatory T cell function. Transcriptome and epitranscriptomic analyses reveal that m6A modification destabilizes Orai1 and Ripk1 mRNAs. Lack of post-transcriptional repression of the encoded proteins correlated with increased store-operated calcium entry (SOCE) activity and diminished survival of T cells. These findings uncover how m6A modification impacts on TCR signal transduction and determines activation and survival of T cells.

Introduction

T cell differentiation, effector function and survival depend on gene expression that is induced during the activation of T cells through their T cell antigen receptor (TCR). For example, immature thymocytes undergo life-or-death decisions in response to signals from the newly rearranged TCR recognizing peptide–major histocompatibility complex (pMHC) conjugates[1], thereby enabling T cell development and TCR repertoire selection[2]. Antigen recognition by peripheral mature T cells enables them to exert effector functions. However, TCR stimulation of these effector T cells can cause activation induced cell death (AICD), which is crucial for the contraction of the expanded peripheral T cell pool that occurs in association with antigen-clearance. In peripheral T cells, cell death mainly occurs through death receptor- or mitochondria-mediated apoptosis pathways[3]. Death receptor-induced apoptosis can be triggered by Fas ligand (FasL) interaction with the Fas receptor, whereas mitochondria-mediated cell death occurs due to loss of mitochondrial membrane potential. Alternatively, death of activated T cells can be regulated by necroptosis[4]. In this pathway Ripk1 and Ripk3 are the key effectors of TNF-induced cell death and mediate apoptosis or necroptosis and inflammation. Downstream of proximal TCR signaling the second messenger Ca^{2+} is induced, allowing amplification and distribution of the signal and leading to profound gene expression changes[5]. Patients with loss-of-function mutations in genes encoding for ORAI1, the main plasma membrane channel for Ca^{2+} influx in lymphocytes, or stromal interaction molecule 1 (Stim1), a critical sensor of Ca^{2+} levels in the endoplasmic reticulum and activator of ORAI1, suffer from immunodeficiency and autoimmunity[6, 7, 8]. Ca^{2+} signaling originates from opening of the Ca^{2+} Release-Activated Ca^{2+} Channel (CRAC) following the activation of STIM1 and STIM2 in the ER membrane, which bind to ORAI1 and ORAI2 proteins that form a Ca^{2+}-permeant pore in the plasma membrane[9]. In T cells this signal ultimately induces nuclear translocation and activation of the nuclear factor and activator of transcription (NFAT), which in turn trans-activates the expression of many effector molecules like cytokines including IL-2 and IFN-g and TNF[10] but also, directly or indirectly, inducing FasL gene

expression thereby imposing AICD[11, 12, 13]. Importantly, excessive Ca^{2+} influx causes cell death by both apoptosis and necroptosis[14], and decreased apoptosis is observed in T cells with impaired intracellular Ca^{2+} mobilization in response to TCR stimulation[8, 15, 16]. Overall, tight regulation of cell death is an important outcome of TCR stimulation and is crucial in maintaining appropriate T cell responses to a stimulus.

In recent years N^6-adenosine methylation-dependent post-transcriptional gene regulation has emerged as a widespread and selective regulatory modification of mRNAs that confers potent control over important cell fate decisions[17, 18]. N^6-methyladenosine (m^6A) has been found to play an essential role in a variety of innate immune responses[19, 20] and to regulate adaptive immunity, where it controls cytokine signaling[21, 22] and is required for early steps of T_{FH} differentiation[23] as well as germinal center B cell formation[24]. However, specific roles in antigen receptor signaling and T cell responses have not been investigated, yet[25]. m^6A modification influences the fate and output of mRNAs by regulating splicing, translation and stability. Emerging evidence has indicated that the modification occurs on selected mRNAs in the context of a DRACH motif (D=G/A/U, R=G/A, H=A/U/C)[18, 26], and is enriched at the stop codon or at the 5' end of the terminal exons that often contain the stop codon. The m^6A modification in mature transcripts has been found to be specifically recognized by cytosolic proteins of the YT521-B homology domain containing (YTHDF) family[17]. The YTHDF1, YTHDF2 and YTHDF3 paralogs bind to the same m^6A-modified mRNAs and act redundantly in inducing mRNA degradation[27, 28]. The m^6A modification is catalyzed by the heterodimeric methyltransferase complex of METTL3 and METTL14[29, 30, 31]. This complex further includes Wilms tumor 1 associated protein (WTAP), RNA binding protein 15 (RBM15/15B), KIAA1429 (VIRMA), ZC3H13 and HAKAI[32, 33, 34]. WTAP is required for the localization of METTL3 and METTL14 within nuclear speckles enriched in mRNA substrates and for the catalytic activity of the m^6A methyltransferase complex *in vivo*[29, 35]. Although METTL3 is the catalytically active component of the METTL3/METTL14 heterodimer, knockdown of either WTAP or VIRMA have been described to cause a similar decrease in cellular mRNA methylation as compared to METTL3 or METTL14 inactivation[29, 36].

A first study addressing the role of m^6A in peripheral T cells[21] showed a requirement for Mettl3 for the proliferation of T cells when transferred into Rag2-deficient mice. The observed lack of activation and proliferation within the lymphopenic host was described as a block of naive T cells to exit quiescence and explained by increased expression of m^6A-modified mRNAs of members of the SOCS family proteins that control the IL-7/STAT5 pathway. In addition, Mettl3 deficiency in Treg cells impaired their suppressive function and caused an inflammatory phenotype, which was similarly explained by upregulation of SOCS protein encoding mRNAs and an expected interference with IL-2/STAT5 signaling in Treg cells[22]. However, also inactivation of Mettl14 in peripheral T cells including conventional and regulatory T cells induced a similar colitis phenotype[37]. While these findings underscored the importance of m^6A modification for Treg cell function, they also posed the question how m^6A-deficient peripheral T cells are involved in the development of colitis[37] if they cannot be activated[21]. To uncover the impact of m^6A modification on

TCR signaling and to unequivocally clarify its role in T cell responses[25], we generated mice with conditional deletion of the essential m^{6}A methylation co-factor Wtap in all T cells or specifically in Treg cells.

Associated with a profound reduction of m^{6}A modification detected on cellular mRNAs, mice with Wtap-deficient T cells or Wtap-deficient Treg cells developed colitis at young age and showed impaired differentiation or maintenance of gut RORγt$^+$ regulatory T cells. Already thymocytes required Wtap function for T cell receptor expression and Wtap deficiency caused impaired differentiation of single-positive CD4 thymocytes in the context of a TCR transgene. Moreover, peripheral T cells lacking Wtap, Virma or Mettl3 exhibited profound AICD. Analyzing m^{6}A modification and Ythdf2 interaction with the transcriptome at near-nucleotide resolution and determining Wtap-dependent changes of mRNA expression, we define Orai1 and Ripk1 as novel m^{6}A-modified and Wtap-repressed targets, overexpression of which caused TCR stimulation-induced cell death. These findings demonstrate a previously unrecognized importance of the m^{6}A methyltransferase complex for the survival of T cells stimulated through their antigen receptor.

Results

Mice with Wtap-deficient T cells develop colitis at young age.

To determine the importance of m^{6}A modification for T cell biology we used mice with conditionally targeted alleles of Wtap, an essential component of the m^{6}A methyltransferase complex. Similar to depletion of Wtap or Mettl3 in various cell lines[29, 36], genetic inactivation of alleles encoding for either of these proteins in primary MEF cells led to a strong reduction of m^{6}A modifications in oligo-dT-purified mRNAs, as determined by quantitative mass spectrometry calibrated with stable isotope labeled internal standards[38] (**Fig. 1a, b**). This confirms the essential function of the Wtap scaffold protein for the activity of the methyltransferase complex. To clarify how Wtap and m^{6}A depletion altered T cell development and homeostasis, we conditionally deleted Wtap encoding alleles in T cells using Cre recombinase expression from the T cell-specific *Cd4* promoter[39] (*Wtap*$^{fl/fl}$; *Cd4*-Cre). Cre expression in thymocytes led to undectable Wtap protein levels in immunoblots (**Extended data Fig. 1a**). Flow cytometry confirmed strongly decreased Wtap expression already in double positive thymocytes and deletion in all CD4 single positive (SP), thymic Treg cells and most CD8 SP thymocytes and peripheral CD4$^+$ and Treg cells, while a small fraction of CD8 SP thymocytes, potentially containing immature thymocytes, still retained Wtap expression (**Extended Fig. 1b**). In this mouse line we observed weight loss and diarrhea in a large fraction of approximately 7 week-old animals lacking Wtap in T cells (**Fig. 1c, d**), consistent with previous findings in mice with genetic inactivation of Mettl14 in T cells[37]. *Wtap*$^{fl/fl}$; *Cd4*-Cre mice developed colitis including reduced colon length and leukocytic infiltration in the colon (**Fig. 1e-g**), and qPCR analysis revealed increased abundance of mRNAs encoding for inflammatory cytokines TNF, IL-1b, IL-2, IL-6, IFN-g and Tgf-*b* in the colon tissue of *Wtap*$^{fl/fl}$; *Cd4*-Cre mice (**Extended data Fig. 1c**). Consistently, CD4$^+$ T cells isolated

from the lamina propria of the colon of these mice produced much more IFN-g or IL-17a. More T cells were also IFN-g and IL-17a double-positive, characterizing them as pathogenic and drivers of T cell-mediated inflammation (**Extended data Fig. 1d, e**). Importantly, the frequencies of RORgt^{+}Helios^{-} induced Treg (iTreg) cells were significantly reduced in the gut of *Wtap*$^{fl/fl}$; *Cd4*-Cre compared to control mice (**Fig. 1h**). To specifically address the function of Wtap in Treg cells, we generated *Wtap*$^{fl/fl}$; *Foxp3-IRES-YFP*-Cre mice[40] (*Wtap*$^{fl/fl}$; *Foxp3*-Cre). Wtap depletion in Treg cells did not affect Treg cell frequencies in the spleen (**Extended data Fig. 1f**), but increased the fraction of CD44^{hi}CD62L^{lo} cells in CD4 and CD8 lineages (**Extended data Fig. 1g, h**) indicating spontaneous activation of peripheral T cells. In the lamina propria of the colon, we found less regulatory T cells and a lower frequency of RORgt^{+}Helios^{-} iTreg cells in *Wtap*$^{fl/fl}$; *Foxp3*-Cre mice compared to control mice (**Fig. 1i, Extended data Fig. 1i**). Interestingly, different from early Cre expression in thymocytes of *Wtap*$^{fl/fl}$; *Cd4*-Cre mice the late expression of Cre in iTreg cells of *Wtap*$^{fl/fl}$; *Foxp3*-Cre mice caused downregulation of RORgt expression, a transcription factor essential for the function of induced Treg cells in the gut[41]. This indicated an instability of gene expression in iTreg cells in addition or causal to the reduction of RORgt^{+}Helios^{-} iTreg cells upon Wtap deficiency in T cells. Cells of the mesenteric lymph node of female *Wtap*$^{fl/fl}$ mice with one *Foxp3-IRES-YFP*-Cre allele revealed the lower frequency of Treg cells with RORgt expression only in Wtap-deficient YFP^{+}Foxp3^{+} as compared to YFP^{-}Foxp3^{+} Treg cells, which are considered wildtype, since they underwent X chromosome inactivation of the *Foxp3-IRES-YFP*-Cre encoding allele (**Extended data Fig. 1j**). These data indicate that under homeostatic conditions, differentiation and stability of Wtap-deficient iTreg cells were impaired in a cell intrinsic manner. Conventional CD4^{+} T or CD4^{+}Foxp3^{+} Treg cells isolated from the lamina propria of the colon from *Wtap*$^{fl/fl}$; *Foxp3*-Cre mice produced more IFN-g or IL-17a compared to wild-type counterparts (**Fig. 1j** and **Extended data Fig. 1k**), further supporting the hypothesis that the function and stability of Wtap-deficient iTreg cells was compromised. Together, these findings demonstrate an essential role for Wtap similar to Mettl3 and Mettl14 in m^{6}A modification and confirm that loss of either of these gene products impairs Treg function and causes inflammation of the gut.

Wtap regulates thymocyte development.

We also tested a role for Wtap in T cell development. Confirming previous findings[21], flow cytometry analysis revealed no significant changes in frequencies and numbers of CD4 SP and Foxp3^{+}CD25^{+} thymocytes (**Fig. 2a, b** and **Extended data Fig. 2a**). However, we observed a clear downregulation of the coreceptor CD8 on CD8 SP thymocytes of *Wtap*$^{fl/fl}$; *Cd4*-Cre mice, also causing a slight decrease in CD8 SP thymocyte numbers (**Fig. 2a, b**). We therefore analyzed maturation of thymocytes determining TCRb and CD24 surface markers. In fact, the TCRb chain showed a decreased expression, which was most pronounced in mature (CD24^{-}) and less evident in immature (CD24^{+}) CD4 SP and CD8 SP thymocytes (**Fig. 2c**). Intracellular staining for TCRb minimized this difference (**Extended data Fig. 2b**), suggesting equal expression but decreased surface localization of the TCR in thymocytes with Wtap-

deficiency compared to wild-type counterparts. Furthermore, mixed bone marrow chimeras with congenically marked *Wtap*$^{fl/fl}$; *Cd4*-Cre (CD45.2^{+}) and wildtype (CD45.1^{+}) bone marrow cells showed similar downregulation of CD8 only in CD45.2^{+} knockout CD8 SP cells indicating a cell-intrinsic effect (**Extended data Fig. 2c, d**).

To demonstrate an influence of Wtap deficiency on thymocyte selection, we generated *Wtap*$^{fl/fl}$; *Cd4*-Cre mice expressing the MHC class I–restricted OT-I[42] or the MHC class II–restricted OT-II[43] TCR transgenes. While the percentage of CD8 SP thymocytes was hardly changed, we again observed downregulation of CD8 on CD8 SP thymocytes from *Wtap*$^{fl/fl}$; *Cd4*-Cre; OT-I mice (**Fig. 2d, e**). Interestingly, *Wtap*$^{fl/fl}$; *Cd4*-Cre; OT-II mice had significantly fewer CD4 SP thymocytes compared to control (**Fig. 2f**). These data indicate altered signaling and selection of OT-II TCR bearing thymocytes lacking Wtap, and suggest that m^{6}A modification may also be important for the generation of a normal T cell receptor repertoire.

The m^{6}A methyltransferase complex is required for T cell survival.

We then questioned whether the colitis phenotype observed after Wtap inactivation in T cells and its impact on thymocyte differentiation also correlated with altered function of conventional T cells in the periphery. Indeed, we found that Wtap-deficient peripheral T cells underwent spontaneous activation as they showed increased percentages of CD44^{hi}CD62L^{lo} CD4^{+} as well as CD8^{+} T cells (**Fig. 3a**). This is different from peripheral Mettl3-deficient CD4^{+} that were described to be locked in a naive state[21]. Surprisingly, the majority of CD62L^{hi} Wtap-deficient CD4^{+} T cells displayed strongly reduced basal expression of the CD44 marker compared to CD44 expression in CD4^{+}CD62L^{hi} cells of wild-type mice (**Fig. 3b**). This direct or indirect regulation of the CD44 marker was confounding for the analysis of naive T cells[21], but did not affect the upregulated CD44 expression in the previously activated CD62^{lo} subset of CD4^{+} T cells (**Fig. 3b**). We found that peripheral CD4^{+} and CD8^{+} T cells were strongly reduced in frequencies and numbers in *Wtap*$^{fl/fl}$; *Cd4*-Cre mice (**Fig. 3c, d**). Similar reduced T cell frequencies were also observed in the knockout compartment of chimeric mice harboring WT (CD45.1^{+}) and *Wtap*$^{fl/fl}$; *Cd4*-Cre (CD45.2^{+}) hematopoetic cells (**Extended data Fig. 3a, b**), and the remaining T cells also showed increased CD44^{hi}CD62L^{lo} percentages for CD4^{+} and CD8^{+} T cell lineages (**Extended data Fig. 3c**). These data show that Wtap deficiency causes the spontaneous activation of CD4^{+} and CD8^{+} T cells and their reduced abundance in a T cell intrinsic manner.

To rule out that these phenotypes were Wtap-dependent but occurred independent of m^{6}A modification, we also analyzed genetic inactivation of Virma, another subunit of the methyltransferase complex, which was similarly required for m^{6}A modification of mRNA (**Extended data Fig. 3d, e** and ref. 36). Consistent with phenotypes occurring upon Wtap inactivation, we found downregulated CD8 expression on CD8 SP and no alteration in frequencies of CD4 SP or Foxp3^{+}CD25^{+} thymocytes in *Virma*$^{fl/fl}$; *Cd4*-Cre mice (**Fig. 3e**, **Extended Data Fig. 3f**). Importantly, we observed similar reductions of peripheral T cells after T cell-

specific inactivation of Virma (**Fig. 3f, g**). Although these phenotypes have not been reported for mice with Mettl3 deficiency in T cells[21, 23], the observed overlap between mice with Wtap or Virma deletion strongly argues for a causal relationship to the lack of m^6A modifications in mRNAs. The differences between Wtap, Virma and the Mettl3 knockouts may therefore relate to different extents of deletion and remaining m^6A marks on mRNAs of T cells in the different conditional knockout mice[19, 44].

Acute deletion of Wtap impairs survival of activated T cells.

Given that *Wtap*$^{fl/fl}$; *Cd4*-Cre mice showed an impairment in thymocyte development and reduction of peripheral T cells, we utilized a *Cd4*-CreERt2 knockin allele[45], and tamoxifen gavage of mice to investigate effects of acute deletion of Wtap in T cells with a normal development and normal TCR repertoire. Flow cytometry analysis one week after last tamoxifen treatment revealed a decreased frequency of $CD4^+$ T cells and reduction in the $CD4^+/CD8^+$ cell ratio (**Fig. 4a, b**) consistent with acute deletion of Wtap encoding alleles only in $CD4^+$ but not $CD8^+$ T cells (**Extended data Fig. 4a**). We next tested how Wtap deficiency affected the persistence of T cells depending on different environments (**Fig. 4c-g**). In lymphopenic *Rag1*$^{-/-}$ mice adoptively transferred T cells undergo homeostatic expansion in response to IL-7 signals as well as TCR-dependent recognition of gut antigens[46]. We transferred $CD45.2^+$ naive $CD4^+$ T cells isolated from control (*Cd4*-CreERt2) or *Wtap*$^{fl/fl}$; *Cd4*-CreERt2 mice into either *Rag1*$^{-/-}$ mice or $CD45.1^+$ congenic wild-type mice. The frequencies as well as numbers of transferred Wtap-depleted $CD4^+$ T cells in the *Rag1*$^{-/-}$ mice were significantly reduced compared to control $CD4^+$ T cells (**Fig. 4d, e**). In contrast, the frequencies and numbers of Wtap-deficient naive $CD4^+$ T cells were only slightly reduced compared to transferred control T cells when they were re-isolated from wild-type $CD45.1^+$ hosts (**Fig. 4f, g**). Flow cytometry analysis confirmed lack of Wtap expression indicating comparable deletion in the adoptively transferred $CD4^+$ T cells reisolated from CD45.1 and *Rag1*$^{-/-}$ mice (**Extended data Fig. 4b, c**). These findings suggested compromised survival or proliferation of T cells with Wtap depletion in lymphopenic hosts, while a much smaller effect was determined for the survival of naive $CD4^+$ T cells in the absence of activation and homeostatic expansion.

To discriminate whether TCR-induced activation compromises the expansion or persistence of Wtap-deficient T cells, we injected anti-CD3 antibodies into mice with wild-type or Wtap-deficient $CD4^+$ T cells (**Fig. 4h**). The cell proliferation marker Ki67 was similarly induced in control and Wtap-depleted $CD4^+$ T cells in response to anti-CD3 injection into mice that had received tamoxifen gavage (**Fig. 4i** and **Extended data Fig. 4d**). However, we found reduced $CD4^+$ T cells numbers in the lymph nodes (LNs) of *Wtap*$^{fl/fl}$; *Cd4*-CreERt2 mice in response to anti-CD3 antibody injection, while PBS-injection did not elicit comparable effects (**Fig. 4j**). In fact, total lymph node cell numbers of control mice increased in response to anti-CD3 antibody injection, while those of *Wtap*$^{fl/fl}$; *Cd4*-CreERt2 mice barely changed (**Extended data**

Fig. 4e). These data suggested an impaired survival of peripheral Wtap-deficient T cells in response to activation and a critical role for m^{6}A modification of mRNAs in TCR-dependent T cell responses.

The m^{6}A methyltransferase complex controls TCR-induced apoptosis.

We next described the fate of T cells undergoing acute deletion of Wtap encoding alleles. Flow cytometry of CD4$^+$ T cells from *Wtap*$^{fl/fl}$; *Cd4*-CreERt2 mice after tamoxifen gavage confirmed depletion of the Wtap protein from naive T cells before stimulation (**Fig. 5a, b**), which had a small inhibitory effect on proliferation after *ex vivo* stimulation (**Fig. 5c**). However, Wtap deletion in conjunction with TCR stimulation strongly induced apoptosis, since the annexinV positive CD4$^+$ T cell population increased from day 2 and accumulated towards day 4 after stimulation (**Fig. 5d**). Consistent results were obtained upon Virma depletion and stimulation of CD4$^+$ T cells (**Extended data Fig. 5a, b**). Interestingly, in the absence of TCR stimulation Wtap-depletion did not alter the viability of naive CD4$^+$ T cell when they were cultured in the presence or absence of IL-7 (**Fig. 5e** and **Extended data Fig. 5c**). IL-7 signaling was intact in T cells from both genotypes, since IL-7 clearly prevented cell death in naive CD4$^+$ T cell cultures from control as well as *Wtap*$^{fl/fl}$; *Cd4*-CreERt2 mice (**Fig. 5e**) that is readily observed without stimulation (**Extended data Fig. 5c**). This indicates that the m^{6}A methyltransferase complex is dispensible for the persistence of naive but becomes essential for the survival of activated T cells stimulated through their TCR.

We confirmed that also sgRNA/Cas9-genome editing in CD4$^+$ T cells interfering with Mettl3 protein expression caused cell death upon TCR re-stimulation (**Fig. 5f, g**). Importantly, depletion of Mettl3 or Wtap in CD4$^+$ T cells did not diminish T cell activation, but rather conferred stronger acute responses to TCR and co-stimulation as deduced from CD69 activation marker expression (**Fig. 5h** and **Extended data Fig. 5d, e** and ref. 23). These findings implicated a stronger TCR induced signal transduction in the death of m^{6}A-deficient T cells.

Identification of m^{6}A-modified and Wtap-regulated mRNAs.

We sought to identify m^{6}A-modified and regulated mRNAs that control TCR signaling and T cell survival. We performed mRNA sequencing from CD4$^+$ wild-type controls and acute *in vitro* deleted Wtap (iKO^T) genotypes. CD4$^+$ T cells were incubated with 4'OH-tamoxifen before stimulation with anti-CD3/anti-CD28 and further expansion in IL-2 (**Extended data Fig. 6a**). We observed full depletion of the Wtap protein on day 4, which caused increased frequencies of apoptotic cells and was associated with a drop of m^{6}A abundance on oligo-dT-purified mRNA as determined by quantitative mass-spectrometry (**Extended data Fig. 6b-d**). We identified 1577 differentially expressed genes (DEG) showing an enrichment of the GO terms immune system process and regulation of apoptotic process in the upregulated DEGs (**Fig. 6a**).

Upregulated DEGs also enriched the GO terms of anti-viral, innate and induced NF-kB responses, consistent with previous work involving m^{6}A function in the prevention of formation and cellular sensing of dsRNA[20]. There was no significantly enriched GO term in the downregulated DEGs (**Fig. 6a**). This suggested that impaired repression of m^{6}A targets after Wtap depletion is responsible for the observed apoptotic phenotype. Indeed, TCR stimulation of CD4$^+$ T cells increased the expression of Ythdf-1/2/3 proteins, the prototypic cytoplasmic m^{6}A-binding and mRNA decay-inducing proteins[47]. Upregulation of Ythdf-1/2/3 proteins was already observed 3-6 hrs after combined anti-CD3/anti-CD28 or PMA/ionomycin stimulations (**Fig. 6b** upper panels) and was recapitulated by PMA but not ionomycin stimulation (**Fig. 6b** lower panels).

We narrowed down DEGs with potential direct regulation by crosslinking and immunoprecipitation experiments using antibodies against m^{6}A (**Fig. 6c**) and Ythdf2 (**Fig. 6d**). We performed cross-linking of m^{6}A-specific antibodies directly bound to mRNA isolated from CD4$^+$ T cells *in vitro*, combined with immunoprecipitation (m^{6}A-CLIP)[48]. We also crosslinked intact CD4$^+$ T cells and performed immunoprecipitation of the cellular Ythdf2 protein on protein extracts (Ythdf2-iCLIP)[49]. Identification of peaks at near-nucleotide resolution was obtained by PureCLIP analyses. This analysis identifies high-density read regions harbouring reoccurring truncations in the sequence reads resulting from protease-resistant peptide adducts at crosslink sites in the RNA that will prematurely terminate the reverse transcription reaction[50]. To determine specific CLIP peaks and distinguish them from background noise, we also prepared libraries using RNA fragments from an identical size range of non-immunoprecipitated samples (size-matched input, SM-Input) and used their sequenced reads to subtract the background. Most m^{6}A-CLIP or Ythdf2-iCLIP-specific peaks were enriched in independent biological replicates, indicating high reproducibility even at the level of identified peaks (**Extended data Fig. 7a**). Our analyses showed that significant peaks were abundant in the 3' UTR and coding region of mRNAs (**Fig. 6c, d**), as previously reported[23, 29]. Overlapping peak regions between the two different CLIP experiments were then defined as Ythdf2 interactions occuring within a window of +/– 20nt around the m^{6}A position, thereby accounting for potential different properties of the m^{6}A-specific antibody or the Ythdf2-protein in the crosslinking step (**Extended data Fig. 7b**). m^{6}A- and Ythdf2-iCLIP experiments showed an overlap of 21,936 peaks present in 3,142 genes (**Fig. 6e).** The majority of these genes overlapped with those encoding for m^{6}A-modified transcripts identified in T_{FH} cells (**Extended data Fig. 7c** and ref. 23). We determined the regulation of genes with overlapping CLIP peaks in the mRNA sequencing of WT and Wtap knockout CD4$^+$ T cells (**Fig. 6f**) and identified an intersection of 281 genes (**Fig. 6g**). Within these 281 mRNAs 188 mRNAs were upregulated (**Fig. 6f**) and included new m^{6}A-regulated target mRNAs like *Orai1*, *Ripk1* together with the known targets *Cish*, *Il2ra*, *Tnf*, *Tnfrsf1b* (**Fig. 6f**), which were previously reported[21, 23, 51]. CLIP-identified sequence reads were typically enriched around the stop codon, at the beginning of the 3'UTR of *Orai1* and *Ripk1* as well as *Cish*, *Tnf* and *Tnfrsf1b* mRNAs and identified overlapping regions with accumulated reads in m^{6}A- and Ythdf2-iCLIP experiments (**Fig. 6h** and **Extended data Fig. 7d**). The identified CLIP peaks in *Ripk1*, *Orai1*, *Cish* and *Tnfrsf1b* also contained DRACH motifs

(**Fig. 6i** and red arrows in **Fig. 6h** and **Extended data Fig. 7d)**. The combination of mRNA- and multiple CLIP-sequencing approaches was therefore able to confirm known targets and identify novel targets in TCR-induced Ca^{2+} signaling and cell death pathways.

Wtap depletion increases expression and stability of *Orai1* and *Ripk1* mRNAs.

We employed qPCR analyses to confirm upregulation of mRNAs encoding for Orai1, Ripk1, Tnf and Tnfr-II (Tnfrsf1b) upon acute deletion of Wtap in $CD4^+$ T cells (**Fig. 7a** and **Extended data Fig. 8a**). In fact, also the mRNA expression encoding for Stim1 and Stim2, activators of ORAI1, was increased in $CD4^+$ T cells with inducible deletion of Wtap (**Extended data Fig. 8a**). The expression of Orai1 and Ripk1 was also increased on the protein level in $CD4^+$ T cells with inducible deletion of Wtap as determined by flow cytometry or immunoblot experiments (**Fig. 7b, c**). Wtap depletion in $CD4^+$ T cells significantly extended the half-life of *Orai1*, *Ripk1* and *Tnfrsf1b* mRNAs in T cells treated with actinomycin D when compared to the respective half-lives in wild-type T cells (**Fig. 7d** and **Extended data Fig. 8b**). Collectively, these data suggest that m^6A mRNA modification of *Orai1*, *Ripk1* and *Tnfrsf1b* mRNAs is essential to determine appropriate expression of these genes in $CD4^+$ T cells.

Wtap controls TCR signal transduction and cell death of T cells.

To demonstrate a functional importance of Wtap and m^6A modification for Ca^{2+} and cell death signaling, we tested store-operated calcium entry (SOCE) in $CD4^+$ T cells. Flow cytometry revealed that Wtap depletion in $CD4^+$ T cells resulted in elevated and more sustained SOCE in ionomycin- or thapsigargin-stimulated T cells compared to control T cells (**Fig. 8a**). Of note, the smaller Ca^{2+} peak observed in reponse to ionomycin stimulation before adding extracellular calcium, which reflects endoplasmic reticulum (ER)-dependent store depletion, was similar in wildtype and iKO T cells (**Fig. 8a**). Consistent with Wtap deletion affecting Orai1 levels, we did not observe changes in proximal TCR signaling when analyzing tyrosine phosphorylation (pTyr) in response to anti-CD3/anti-CD28 stimulation (**Fig. 8b**). Since Ca^{2+} influx leads to the activation of several transcription factors in T cells, we investigated the phosphorylation of NFAT and CREB proteins as well as c-Fos following ionomycin stimulation (**Fig. 8c**). Basal expression and dephosphorylation of NFAT1 and NFAT2 after ionomycin stimulation was enhanced in iKO compared to control $CD4^+$ T cells (**Fig. 8c**). In addition, we observed increased phosphorylation of CREB (S133-P) and strongly induced expression of c-Fos protein as well as Egr1-3 mRNAs associated with the increased Ca^{2+} signaling in iKO $CD4^+$ T cells (**Fig. 8c, d**). Consistent with the *Fasl* gene being a target of NFAT and Egr transcription factors[11, 12, 13], elevated Ca^{2+}/NFAT/Egr activation in $CD4^+$ T cells with Wtap depletion correlated with increased expression of FasL protein after anti-CD3/anti-CD28 stimulation (**Fig. 8e**).

We then employed retroviral transduction of T cells to assess the link between Orai1 or Ripk1 overexpression and cell death. Transduction of activated $CD4^+$ T cells with retroviruses harboring ORAI1 or Ripk1 cDNAs marked by IRES-dependent Thy1.1 expression was associated with reduced viability of the transduced T cells upon re-stimulation with anti-CD3/anti-CD28 when compared to cells expressing Thy1.1 from eGFP encoding vector (**Fig 8f-i**). These data demonstrate that increased ORAI1 or Ripk1 expression can cause cell death in T cells in the context of TCR signaling.

Finally, we utilized the small molecule inhibitors zVAD-fmk or Nec-1 to assign the relative contributions of apoptosis and necroptosis to reduced survival of TCR-stimulated Wtap-deficient $CD4^+$ T cells. Importantly, zVAD-fmk and Nec-1 treatments synergized in the rescue of viability, suggesting an involvement of both apoptosis and necroptosis in observed TCR-induced death of Wtap-deficient T cells (**Fig. 8j**).

These findings therefore demonstrate that the m^6A methylation of *Orai1* and *Ripk1* mRNAs provides $CD4^+$ T cells with regulatory mechanisms to control cell death pathways affecting T cell survival following TCR stimulation.

Discussion

Several reports revealed that epitranscriptomic regulation impinges on adaptive immune responses[23] and specifically on the biology of mature T cells[21] and regulatory T cells[22, 37]. However, important questions as to where in the T cell transcriptome m^6A modifications are positioned[19, 47, 52], whether these modifications impact on thymocyte development[19] and whether they rather affect IL-7 or TCR signal transduction in mature T cells[25] remained unanswered. It also appears important to further analyze m^6A modification by genetic inactivation of different components of the methyltransferase complex, since ablation of Mettl3 with different Cre-lines, including CD4-, CD11c- or Foxp3-Cre, only partially reduced the m^6A marks on mRNAs[19] and could therefore not give a complete picture of m^6A controlled phenotypes.

We used conditional gene targeting of Wtap, an essential scaffold protein of the m^6A methyltransferase complex. We determine undetectable Wtap protein expression in thymocytes and peripheral T cells following CD4-Cre mediated deletion, and complete deletion of Wtap exemplified in MEF cells wiped out m^6A marks. Deficiency of Wtap impaired the functionality of Treg cells, especially of $RORgt^+$ induced Treg cells in the gut, causing a colitis phenotype that was consistent with the phenotypes of Mettl3 or Mettl14 ablation. In contrast, other phenotypes of Wtap deficiency in T cells differed significantly from Mettl3 targeting, since conditional deletion of Wtap with CD4-Cre downregulated CD8 coreceptor and TCRb expression in SP thymocytes. Moreover, introducing a fixed antigen receptor by crossing $Wtap^{fl/fl}$; CD4-Cre mice with TCR transgenic mice revealed that the m^6A methyltransferase complex participates in TCR repertoire selection likely by modulating TCR signaling or TCR internalization in thymocytes. Importantly, conditional or induced deletion of Wtap alleles in peripheral T cells strongly compromised survival in the context of TCR signal transduction.

The WTAP protein is also present in another complex with the Wilms tumor 1 (WT1) protein, which was proposed to control alternative splicing of selective targets through a versatile interaction of WT1 with RNA, with other proteins, as well as with DNA[53]. Nevertheless, these m^6A-independent functions of Wtap are unlikely to cause the phenotypes reported here, since they were recapitulated by conditional gene targeting of Virma, which has only been involved in shared functions with Wtap in the m^6A methytransferase complex.

In this study, we provide a map of m^6A modifications presenting m^6A and Ythdf2 iCLIP results for the transcriptome of mouse $CD4^+$ T cells at near-nucleotide resolution. YTHDF proteins contain only one discernable folded domain of the YT521-B Homology family type that is known to specifically interact with m^6A modification on RNA[27]. We propose that the overlap of both approaches provides confidence for *in vivo* modified sites that are accessible and able to contribute to post-transcriptional gene regulation. We describe a strong effect of Wtap deletion during TCR activation causing AICD, and under these conditions, the expression of cellular Ythdf proteins strongly increased. Since the GO term of apopotic processes was associated with upregulated mRNAs of Wtap knockout T cells, it suggested a regulation of apoptosis-relevant mRNAs by prototypic Ythdf m^6A readers because these target mRNAs for decay. Key m^6A-modified and Wtap-repressed targets that our work has involved in the activation induced death of T cells were the Ca^{2+} channel Orai1 and the programmed cell death inducing kinase Ripk1.

Ca^{2+} signaling determines many different aspects of T cell fate decisions not only effector functions but also AICD[5, 54]. In fact, $CD4^+$ T cells lacking ORAI1 revealed reduced AICD and enhanced survival[15, 16]. As we show here, Wtap depletion caused upregulation of Orai1, led to enhanced and more sustained Ca^{2+} signaling, and overexpression of ORAI1 was able to increase TCR induced death of T cells. We find that elevated Ca^{2+} signals in Wtap-deficient T cells also enhanced the expression of the Egr1,2,3 encoding mRNAs. In addition to their regulation of the Fas ligand gene with critical importance for AICD[12] these transcription factors directly bind and transactivate SOCS1 and SOCS3 promoters[55]. We therefore expect that there are Ca^{2+} dependent contributions to the increased expression of SOCS genes[21] and potential impact on cytokine signal transduction. However, we did not determine a significant change in IL-7 induced survival of naive T cells upon genetic inactivation of Wtap.

Ripk1, another previously unrecognized target of the m^6A methyltransferase complex, was also upregulated after Wtap depletion. Ripk1 has important kinase-dependent and scaffolding functions and can trigger either necroptosis or apoptosis under different conditions depending on the functional activity of Caspase 8 (ref. 4). Interestingly, the observed cell death that occured in response to T cell activation in Wtap-deficient T cells was rescued partially by both zVAD-fmk and Nec-1 revealing similar contributions from caspase- and RIP1-dependent cell death pathways. Future work will have to define whether these m^6A targets involved in cytokine signaling, Ca^{2+} signaling and T cell death by apoptosis or necroptosis or regulation of other mRNA by m^6A is responsible for the control of thymocyte development and Treg cell function.

In summary, our studies link the m^{6}A methyltransferase complex to crucial control of TCR-dependent T cell activation and survival. Given that m^{6}A modifications are observed only in specific subsets of mRNAs and and can be bound by different reader proteins, each cell type may establish unique regulatory networks. Starting with a knowledge of the transcriptome-wide m^{6}A marks in CD4$^+$ T cells, it will be important to discriminate how different m^{6}A readers and other RNA-binding proteins cooperate to arrive at context-dependent responses for example the balancing of activation and death of T cells, the selection of thymocyte and establishment or maintenance of Treg cell identity.

Methods

Mice.

Wtap$^{f/lfl}$ mice and *Virma*$^{fl/fl}$ mice were obtained from the European Conditional Mouse Mutagenesis Consortium (EUCOMM, https://www.mousephenotype.org/data/genes/MGI:1926395 and https://www.mousephenotype.org/data/genes/MGI:1913435). To generate mice with T cell-specific *Wtap* or *Virma* deficiency as well as Treg cell-specific *Wtap* deficiency, mice were crossed with *Cd4*-Cre[39] or *Cd4*-Cre-ERt2[45], or *Foxp3*-IRES-*YFP*-Cre[40]. The MHC class I or II-restricted transgenic TCR was introduced by crossing mice to the OT-I line[42] or OT-II line[43]. *Rag1*$^{-/-}$ mice and mice expressing CD45.1 (Ptprca Pepcb/BoyJ) were from Jackson Laboratory. All mice were bred and maintained under specific pathogen-free conditions and all experiments were performed in accordance with Helmholtz Zentrum München and the Ludwig-Maximilians-Universität institutional, state and federal guidelines. All experimental procedures involving mice were performed in accordance with the regulations of and were approved by the local government (Regierung von Oberbayern).

In vitro and *in vivo* deletion of Wtap or Virma encoding genes.

For *in vitro* deletion in T cells, total CD4$^+$ T cells mice were isolated from spleen and lymph nodes using the EasySep^{TM} Mouse CD4$^+$ T cell Isolation Kit (STEMCELL) according to the manufacturer's protocol. Purified CD4$^+$ T cells were cultured in DMEM (Invitrogen) cell culture medium supplemented with 10% FCS (Gibco), 100U Pen-Strep (Thermo Fisher), 10 mM HEPES-Buffer (Invitrogen), 1% non-essential amino acids (NEAA; Invitrogen) and 50 µM b-mercaptoethanol (Invitrogen). For activation and differentiation, T cells were stimulated with anti-CD3 (1 µg/mL; cl. 145-2C11, in house production), anti-CD28 (2.5 µg/mL; cl. 37.5N, in house production) under Th1 conditions, 10 µg/mL α-IL-4 (cl. 11B11, in house production) and 10 ng/mL IL-12 (BD Pharmingen) and cultured on six-well plates pre-coated with goat anti-hamster IgG (50 µg/mL, MP Biochemicals) for 40-48h at an initial cell density of 5×10^6 cells/mL. For Wtap depletion, T cells were treated with 1 µM 4' OH-tamoxifen (Sigma) for 24 h prior to the activation. Following stimulation cells were resuspended in T cell medium supplemented with 200 IU/mL

recombinant hIL-2 (Novartis) and expanded in an incubator with 10% CO_2. Every 24h the cells were diluted to a density of 1×10^6 cells/mL in IL-2-containing medium.

For *in vivo* deletion, mice were orally gavaged with 5 mg tamoxifen in 150 µL corn oil per mouse twice a day on 2 consecutive days. The mice were sacrificed three days after the last gavage and naive $CD4^+$ T cells were isolated using the EasySep^{TM} Mouse naive $CD4^+$ T cell Isolation Kit (STEMCELL) according to the manufacturer's protocol.

Transfection and viral transduction

cDNAs encoding hORAI1, Ripk1 or eGFP were PCR amplified and inserted into a mouse stem cell virus (MSCV) retroviral vector containing an internal ribosome entry site (IRES)-Thy1.1 cassette (Addgene). Calcium-phosphate transfection was used to generate retroviral particles. In brief, HEK293T cells were seeded at a density of 7×10^6 cells on 15 cm culture dishes one day prior to transfection in DMEM medium (Invitrogen) supplemented with 10% (v/v) FCS (Gibco), 100U Pen-Strep (Thermo Fisher), 10 mM HEPES-Buffer (Invitrogen), 1% non-essential amino acids (NEAA; Invitrogen) at 37°C and 10% CO_2. On the day of transfection, HEK293T cells were pre-treated with 25 µM chloroquine for 1h and were then cotransfected with 5µg of the packaging vector pCL-Eco (Addgene; 12371) and 50 µg of the pMSCV plasmids using calcium phosphate as a transfection reagent. After 6 h the medium was replaced with fresh medium for an additional 48 h. Viral particles were collected, filtered (0.45 µM) and mixed with polybrene (10 µg/mL) prior to spin-infection. Retroviral transduction was performed 40h after the start of anti-CD3/CD28 activation under T_H1 conditions using spin-inoculation (1h, 18°C, 850g). After 4-6h of co-incubation of T cells with virus, virus particles were removed and T cells resuspended in T cell medium supplemented with IL-2. T cells were re-stimulated with anti-CD3/CD28 antibodies.

Flow cytometry analysis.

Single-cell suspensions were stained with LIVE/DEAD Fixable dye in PBS for 20 min at 4 ºC. For the detection of surface markers, cells were stained with antibodies in FACS buffer (2% FCS, 1mM EDTA in PBS) for 30 min at 4 ºC. If needed, cells were fixed and permeabilized for intracellular staining. For intracellular staining of Foxp3, RORgt, Helios, METTL3, WTAP and VIRMA T cells were fixed and permeabilized using the Foxp3/Transcription Factor Staining buffer set (eBioscience) according to the manufacturer's instructions. To detect the WTAP, VIRMA and METTL3 proteins, a secondary goat anti-mouse Ig conjugated with FITC or APC (BD) or a secondary goat anti-rabbit Ig conjugated with Alexa Fluor 647 or APC antibodies (Invitrogen) were used. To maintain the YFP signals during intracellular staining, samples were fixed in 1% paraformaldehyde in PBS for 15 min at room temperature.

For intracellular cytokine staining, $CD4^+$ T cells were stimulated with PMA (20 nM) and ionomycin (1 µM) for 4 hr and Brefeldin A (10 µg/ml) was added during the last 2 hr. Subsequently, LIVE/DEAD staining was performed followed by fixation for 15 min at room temperature with 2% formaldehyde. Cells were permeabilized and stained with antibodies for 40 min at room temperature in PBS containing 0.5% saponin and 1% BSA. For staining of ORAI1, cells were fixed in 4% paraformaldehyde for 10 min at room temperature and permeabilized for 30 min using the Permeabilization Buffer of the Foxp3/Transcription Factor Staining buffer set (eBioscience). Cells were then stained with the antibody in the Foxp3 Permeabilization Buffer for 30 min at room temperature. To detect the ORAI1 antibody a secondary goat-anti-rabbit Alex488 antibody was applied. After staining, cells were acquired on a FACS LSR Fortessa (BD Biosciences) or FACS Canto II (BD Biosciences) device and samples were analyzed with FlowJo software.

Antibodies.

For flow cytometroy analysis, the following antibodies were used: anti-CD4 (cl. GK1.5), anti-CD8a (cl. 53-6.7), anti-TCRb (cl. H57.597), anti-CD25 (cl. PC61.5), anti-Va2 (cl. B20.1), anti-CD62L (cl. MEL-14), anti-CD45.1 (cl. A20), anti-CD45.2 (cl. 104), anti-Foxp3 (cl. FJK-16S), anti-Ki67 (cl. SolA15), anti-CD90.1 (cl. HIS51) were from eBioscience. anti-CD24 (cl. M1/69), anti-CD44 (cl. IM7), anti-IFN-γ (cl. XMG1.2), anti-IL-17A (cl. TC11-18H10.1), anti-Helios (cl. 22F6), anti-FasL (cl. MFL3), anti-phosphoTyr-APC (PY20) were from BioLegend. anti-Rorgt (cl. Q31-378) was from BD Biosciences. anti-ORAI1 (YZ6596, in house production). For Immunoblot analysis, the following antibodies were used: anti-YTHDFs (cl. 17F2, in house production). anti-RIP1 (cl. D94C12), anti-NFAT1 (cl.D43B1), anti-NFAT2 (cl. D15F1), anti-pCREB (S133) (cl. 87G3), anti-c-Fos (cl. 9F6) were from Cell signaling. anti-GAPDH (6C5) was from Merck Millipore. Anti-METTL3 (cl. EPR18810, abcam), anti-WTAP (cl. 4A10G9, Proteintech), anti-VIRMA (cl. D4N8B, Cell signaling) were used.

Quantitative RT-PCR analyses with reverse transcription

Total RNA was isolated with the NucleoSpin RNA kit (Macherey-Nagel) or by phenol-chloroform extraction method using Trizol (Ambion). cDNA was synthesized from 0.5-1 µg of total RNA with RevertAid Reverse Transcriptase (Thermo Fisher Scientific, Waltham, MA, USA). Quantitative RT-PCR analyses were performed using Light Cycler 480 Probes Master Mix and primer-/probe-combinations from Roches Universal Probe Library (Roche). PCR reactions were run on a Roche Light Cycler 480II machine. Relative gene expression was normalized to the expression of the housekeeping gene Ywhaz. For mRNA decay assays, $CD4^+$ T cells were treated with 5 µg/ml actinomycin D to stop newly synthesized mRNA. Samples were collected at different time points after Actinomycin D addition. Primers used for the quantitative RT-PCR are described in Supplementary Table 1.

Immunoblot analysis.

Cells were lysed in lysis buffer (20 mM Tris-HCl, pH 7.5, 150 mM NaCl, 0.25% (v/v) Nonidet-P40, 1.5 mM $MgCl_2$ supplemented with 1x cOmplete, EDTA-free Protease Inhibitor Cocktail (Roche) on ice for 15 min. After centrifugation for 15 min at 12.000 g, protein concentrations were measured using the Bio-Rad protein assay. Cell lysates denatured in 3x SDS sample buffer (150 mM Tris-HCl, 6% SDS, 20% glycerol, 6 mM EDTA, 5% b-Mercaptoethanol, bromophenol blue) were separated by SDS polyacrylamide gel electrophoresis (SDS-PAGE) and transferred to polyvinylidene difluoride (PVDF) membranes (Immobilon P, Merck Millipore). Membranes were then incubated with primary antibodies. Immunoreactive proteins were visualized with horseradish peroxidase (HRP)-conjugated secondary antibodies (Cell Signaling), which was followed by processing with an ECL detection system and X-ray films were used.

AnnexinV staining.

Single-cell suspensions were stained with LIVE/DEAD Fixable dye in PBS for 20 min at 4 ºC. Then Cells were stained with the fluorochrome-conjugated Annexin V (eBioscience) by using the Annexin V apoptosis detection kit according to manufacturer's instructions (eBioscience). zVAD-fmk (BD Bioscience) and Nec-1 (Calbiochem) were used at 40 µM and 10 µM, respectively.

Cell proliferation assay and Naive T cell Culture.

Naive $CD4^+$ T cells from *Cd4*-CreERt2 and *Wtap*$^{fl/fl}$*Cd4*-CreERt2 mice that had received tamoxifen gavage were isolated using the EasySep™ Naïve $CD4^+$ T Cell Isolation Kit (STEMCELL) according to manufacturers' instructions. Isolated cells were labelled with CellTrace™ Violet dye in sterile PBS supplemented with 0.1% FBS for 20 min at 37 ºC according to manufacturers' instructions. Naive T cells were stimulated with anti-CD3/CD28 antibodies. For naive T cell culture, cells were cultured in RPMI1640 (Invitrogen) T cell culture medium supplemented with 10% FCS (Gibco), 100U Pen-Strep (Thermo Fisher), 10 mM HEPES-Buffer (Invitrogen), 1% non-essential amino acids (NEAA; Invitrogen), 50 µM b-mercaptoethanol (Invitrogen) and 20 ng/mL recombinant IL-7 (Novartis).

Measurement of Ca^{2+} influx.

Single-cell suspensions were stained with LIVE/DEAD Fixable dye in PBS for 20 min at 4 ºC. Then cells were labelled with 1 µM Fluo-4-AM and 1 µM FuraRed for 30 min at room temperature in T cell medium which was followed by 2 wash steps with Ca^{2+}-free Ringer solution (155 mM NaCl, 4.5 mM KCl, 3 mM $MgCl_2$, 10 mM D-glucose and 5 mM Na-HEPES). Changes in intracellular Ca^{2+} concentrations were analyzed using a FACS LSR Fortessa (BD Biosciences) at 488 and 630 nm excitation wavelengths. Cells

were stimulated with 1 µM thapsigargin or 1 µM ionomycin in Ca^{2+}-free Ringer solution and SOCE was analyzed after readdition of 2 mM Ca^{2+} Ringer solution (155 mM NaCl, 4.5 mM KCl, 1 mM $MgCl_2$, 2 mM $CaCl_2$, 10 mM D-glucose and 5 mM Na-HEPES).

Adoptive naive $CD4^+$ T cells transfer.

Naive $CD4^+$ T cells were isolated from donor mice using the EasySep™ Naïve $CD4^+$ T Cell Isolation Kit (STEMCELL) according to the manufacturers' instructions. Isolated cells were resuspended in sterile PBS and purity was confirmed by flow cytometry. $2x10^6$ cells were injected i.v. into $CD45.1^+$ or *Rag1*$^{-/-}$ recipient mice. On day 1 and 2 post injection all recipient mice were given 5mg tamoxifen by oral gavage twice per day (20mg total tamoxifen per mouse). Recipient mice were sacrificed seven days after receiving the last tamoxifen gavage.

Generation of mixed bone marrow chimeras.

Bone marrow cells collected from congenic C57BL/6 ($CD45.1^+$) mice were mixed at a ratio of 1:1 with bone marrow cells from $CD45.2^+$ mice and the mixture (4-5 x 10^6) was injected into the tail vein of irradiated CD45.1/2 heterozygous recipient mice (550 rads). Mice were treated for two weeks with water supplemented with antibiotics and mice were analyzed 7-8 weeks after the transfer.

Isolation of lymphocytes from the lamina propria.

Mice were sacrificed and colons were removed and flushed with ice cold PBS. Colons were cut into small pieces, pre-digested in HBSS supplemented with 8% FCS, 10 mM HEPES, 10 mM EDTA followed by three digestions in HBSS supplemented with 8% FCS, Collagenase Type IV (157 U/ml, Sigma), DNase I (0.2 mg/ml, Roche) and Liberase DH (0.125 mg/ml, Roche) for 1h. Lymphocytes were purified using a 40/80 Percoll gradient (GE Healthcare). Purified lymphocytes were stained with LIVE/DEAD Fixable dye followed by surface staining and intracellular staining.

Detection of TCR-induced tyrosine phosphorylation.

$CD4^+$ T cells were stimulated with anti-CD3/CD28 antibodies and crosslinked with goat anti-hamster IgG at indicated times. Cells were washed with FACS buffer and fixed with BD Phosflow™ Lyse/Fix Buffer (BD Bioscience) at 37 ºC, 10 min, which was followed by permeabilization by using the BD Phosflow™ Perm Buffer III (BD Bioscience) at 4 ºC, 30 min according to the manufacturer's instructions. Cells were

washed and stained with anti-phosphoTyr-APC (BioLegend) in FACS buffer at room temperature for 30 min. Flow cytometry was performed using a FACS Canto II (BD Biosciences).

Generation and culture of Mettl3 knockout T cells.

Total $CD4^+$ T cells mice were isolated from spleen and lymph nodes using the $CD4^+$ T Cell Isolation Kit, mouse (Miltenyi Biotec) according to manufacturer's protocol. Purified $CD4^+$ T cells were cultured in RPMI1640 (Invitrogen) T cell culture medium supplemented with 10% FCS (Gibco), 100U Pen-Strep (Thermo Fisher), 1% non-essential amino acids (NEAA; Invitrogen), 1% sodium pyruvate, 1% glutamine and 50 µM b-mercaptoethanol (Invitrogen). For activation and differentiation, T cells were cultured on plates pre-coated with anti-CD3 (1 µg/mL; cl. 145-2C11, Thermo Fisher), anti-CD28 (2.5 µg/mL; cl. 37.51, BioLegend) for 48h. The Neon™ Transfection System (Thermo Fisher) was used for the delivery of Cas9 (Thermo Fisher) /gRNA complexes according to manufacturer's protocol. Cells were washed with DPBS and suspended in buffer T and Electroporation Enhancer (IDT). Then cells were mixed with the Cas9/gRNA complexes and electroporated with 1900V, 10 ms, 1 pulse. After 4 days of the transfection, cells were re-stimulated with anti-CD3 (8 µg/mL)/anti-CD28 (4 µg/mL). sgRNAs used for the electroporation are: GGACACGTGGAGCTCTATCC and GATGGGGTAACCAACAATCG for *Mettl3* and GGCGAAGGTTTTGGTTCACC and CGTGTGCTCGGGTATCCCAA for *cd90.1*.

Generation of immortalized Mouse Embryonic Fibroblast (MEF) cells.

MEF cells derived from different embryos were cultured in Dulbecco's Modified Eagle's Medium (DMEM) (GIBCO) supplemented with 10% FCS (Gibco), 100U Pen-Strep (Thermo Fisher), 10 mM HEPES-Buffer (Invitrogen) and 1% non-essential amino acids (NEAA; Invitrogen) at 37°C in 10% CO_2 and immortalized by retroviral transduction with Large T-antigen. Retroviral (MSCV-SV40 Large T-antigen) transduction was performed using spin-infection (1.5h, 32 °C, 300g). Two days after virus infection, cells were passaged and cultured in the presence of Hygromycin B (100 µg/mL) for an additional 3 days to select infected cell populations. To establish *Wtap*$^{-/-}$ or *Virma*$^{-/-}$ MEF cells, retroviral (empty MSCV or MSCV-Cre) transduction was performed. Two days after virus infection, cells were cultured in the presence of puromycin (1.25 µg/mL) for an additional 3 days. To establish *Mettl3*$^{-/-}$ MEF cells, the Neon™ Transfection System (Thermo Fisher) was used for the delivery of Cas9 (Thermo Fisher) /gRNA complexes according to manufacturer's protocol. Cells were washed with DPBS and suspended in buffer R. Then cells were mixed with the Cas9/gRNA complexes and electroporated with 1650V, 20 ms, 1 pulse. After 7 days of the transfection, RNAs and Proteins were isolated. sgRNAs used for the electroporation are: GGACACGTGGAGCTCTATCC and GATGGGGTAACCAACAATCG for *Mettl3* and GGTTCTTGACTACCGTAATT for scrambled control.

m^{6}A-CLIP.

m^{6}A-CLIP experiments were performed as previously described[48]. Total RNA was isolated with TRIzol. For mRNA purification, two rounds of poly(A) selection were perfomed using Dynabeads mRNA purification kit (Ambion) according to the manufacturer's instructions, which was followed by fragmentation using RNA fragmentation reagents (5 min at 70 ºC, 0.1x diluted reagents, Invitrogen). To verify the size of fragmented mRNAs, the mRNA samples were analyzed with the Agilent RNA 6000 pico kit on an Agilent 2100 Bioanalyzer System. The fragmented mRNA samples were incubated with 6 µg anti-m^{6}A antibody (Synaptic Systems) in IP buffer (50 mM Tris-HCl [pH 7.4], 100 mM NaCl, 0.05% NP-40) for 4 hr at 4 ºC and cross-linked twice with 150 mJ/cm^2 UV light (254 nm) in a Stratalinker. After cross-linking, the solution was further incubated with 50 µl of washed protein A beads for 1 hr at 4 ºC, rotating. Bead-bound antibody-RNA complexes were then recovered on a magnetic stand (Life Technologies) and washed twice with high-salt buffer (50 mM Tris-HCl [pH 7.4], 1 M NaCl, 1 mM EDTA, 1% IGEPAL CA-630, 0.1 % SDS, 0.5 % Sodium deoxycholate) and twice with polynucleotide kinase (PNK) wash buffer (20 mM Tris-HCl [pH 7.4], 10 mM $MgCl_2$, 0.2 % Tween 20). RNA 3' ends were dephosphorylated on beads with PNK for 20 min in dephosphorylation buffer (350 mM Tris-HCl [pH 6.5], 5 mM $MgCl_2$, 5 mM DTT). After washing (once with PNK wash buffer, once with high-salt buffer, and twice with PNK wash buffer), the 3' adaptor was ligated with T4 RNA ligase in Ligation buffer (200 mM Tris-HCl [pH 7.8], 40 mM $MgCl_2$, 4 mM DTT) overnight. The samples were radioactively end-labled and eluted from beads with 4 x NuPAGE LDS loading buffer (Invitorgen) containing 50 mM DTT at 70 ºC for 5 min. Then the samples were subjected to NuPAGE gel electrophoresis and tranferred onto a Protan BA85 Nitrocellulose Membrane (Whatman). Membrane regions containing RNA cross-linked antibody heavy and light chains were excised and the RNA was isolated from the membrane by treatment with proteinase K. After phonol/chloroform extraction and precipitation, the RNA was reversed transcribed with SuperScript IV reverse transcriptase (Invitrogen) according to manufacturer's instructions, which is followed by wash with Dynabeads MyOne Silane (Invitrogen). The 5' adaptor was ligated with T4 RNA ligase High concentration (NEB) overnight. First-strand cDNA was synthesized with Phusion High Fidelity PCR Master Mix (NEB) and size-selected using ProNex Size-Selective Purification System (Promega). Libraries were PCR amplified for 18–21 cycles and sequencing with a length of 50 bp, single-read and 40×10^6 reads/sample was performed on a Illumina HiSeq1500 sequencer.

Ythfd2-iCLIP.

Ythdf2-iCLIP experiment was performed as previously described[49]. Cells were washed once with PBS and cross-linked twice with 200 mJ/cm^2 UV light (254 nm) in a Stratalinker. After cross-linking, cells were harvested in PBS and snap freezed in liquid nitrogen and stored at -80 ºC until use. Cells were lysed in lysis buffer (50 mM Tris-HCl, pH 7.5, 100 mM NaCl, 1% (v/v) Igepal CA-630, 0.1% SDS, 0.5% Sodium deoxycholate supplemented with 1x cOmplete, EDTA-free Protease Inhibitor Cocktail (Roche) on ice for 15

min. Protein concentrations were measured by Bradford assay and partial RNA digestion was perfomed by using optimized RNase I dilution (Ambion) together with Turbo DNase (Ambion) at 37 ºC for 3 min. After centrifugation for 10 min at 21,000 g, cell lysates were loaded onto a Proteus Clarification Mini Spin Column (Generon) and spun at 4°C at 16,000 g for 1 min. 50 µl Protein-A dynabeads (Invitrogen) were coupled under constant rotation to 6 µg YTHDF2 antibody (Proteintech) in lysis buffer at 4°C over-night. After washing of the antibody-coupled beads with high-salt buffer (50 mM Tris-HCl [pH 7.4], 1 M NaCl, 1 mM EDTA, 1% IGEPAL CA-630, 0.1 % SDS, 0.5 % Sodium deoxycholate) and lysis buffer, washed beads were incubated with protein lysates in 1 ml lysis buffer for 4h at 4 ºC. Following process and library preparation were perfomed as m^6A-CLIP.

CLIP read processing.

Data processing was done as previously described[56]. Reads were de-multiplexed based on the experimental barcode and adapter sequences were removed from the read ends (Flexbar v3.5.0). UMIs were trimmed and added to the read names. Individual samples were mapped to the respective genome (assembly version GRCm38.p6 for all mouse samples) and its annotation (GENCODE release M25 for all mouse samples) using STAR (v2.7.6a). Reads were de-duplicated if they had identical UMIs. For both m^6A-CLIP and Ythdf2-iCLIP significant crosslink sites at single-nucleotide resolution were called using PureCLIP (v1.3.1) with default parameters, and individual crosslink sites within a distance of 8 bps from each other were merged into wider binding regions (peaks). For assigning a host gene to each PureCLIP peak, transcript annotations were taken from GENCODE release M25, mm10. To intersect peaks from m^6A-CLIP and Ythdf2-iCLIP, each PureCLIP peak region was extended 20 nt on both sides.

RNA-seq and read processing.

$CD4^+$ T cells were incubated with 4'OH-tamoxifen before stimulation with anti-CD3/anti-CD28 and further expansion in IL-2. Total RNA was isolated with the NucleoSpin RNA kit (Macherey-Nagel). Library preparation was performed using SENSE mRNA-Seq Library Prep Kit V2 (LEXOGEN). The libraries were sequenced with a length of 50 bp, paired-end and 20×10^6 reads/sample on an Illumina HiSeq1500 sequencer. Trimmed RNA-seq reads were pseudoaligned to the ENSEMBL GRCm38 Mus musculus release 99 transcriptome using kallisto[57], version 0.44.0. Transcript abundances were quantified using default k-mer length 31. Genes differentially expressed between the two conditions were identified using the R statistical package DESeq2 (ref. 58), which uses linear modeling to test for each gene the null hypothesis that the log2-fold change between the two conditions is 0. We identified significantly differentially expressed genes at a false discovery rate of 0.05 and applied a fold change threshold of 1.5.

Liquid Chromatography Mass Spectrometry for measurement of m^6A abundance.

Total RNA was isolated with TRIzol. mRNAs were purified using Dynabeads mRNA purification kit (Ambion) according to manufacturer's instructions. Samples were subjected to rRNA depletion with the RiboMinus Transcriptome Kit (Invitrogen) and again purified using the Dynabeads mRNA purification kit. To verify the size of fragmented mRNAs, the mRNA was analyzed with the Agilent RNA 6000 pico kit on an Agilent 2100 Bioanalyzer System. For nucleoside quantification a 1290 Infinity II (Agilent Technologies, Waldbronn, Germany) equipped with a diode array detector (DAD) combined with a G6470A Triple Quad system (Agilent Technologies) and electro-spray ionization mass spectrometry (ESI-MS, Agilent Jetstream; Agilent Technologies) was used with operating parameters as previously described[38]. The instrument was operated in dynamic multiple reaction monitoring (MRM) mode. The mobile phases were: A as 5 mM NH_4OAc (≥99%, HiPerSolv CHROMANORM®, VWR) pH = 5.6 aqueous buffer and B as pure acetonitrile (Roth, liquid chromatography–mass spectrometry (LC–MS) grade, purity ≥ 99.95). A Synergi Fusion-RP column (Phenomenex®, Torrance, CA, USA; Synergi® 2.5 µm Fusion-RP 100Å, 150 × 2.0 mm) at 35 ºC and a flow rate of 0.35 mL/min was used. The gradient started with 100% A for one minute, increased to 10% B by 5 min, and to 40% B by 7 min with a one minute 40% B flushed before returning to 100% A by 8.5 min and held for 2.5 additional minutes.

Statistical Analysis.

Statistical analysis was performed with Prism 5.0c (GraphPad). *P* values were calculated with Student's *t* test or two-way ANOVA test, as indicated. Error bars represent mean of all data points with +/- SEM.

Declarations

Acknowledgments.

We thank Claudia Keplinger (Helmholtz Zentrum München) and Lena Esser (Ludwig Maximilian Universität) for excellent technical support. We thank the BMC Core Facility (Ludwig Maximilian Universität) for flow cytometry, Helmut Blum and Stefan Krebs (Ludwig Maximilian Universität) for mRNA and CLIP sequencing and Nick Angstman for initial processing of sequencing data. This study was supported by the German Research Foundation grants HE3359/8-1, HE3359/7-1 and SFB 1054 (project A03), SPP 1935 and TRR338 (project C02) to V.H.

AUTHOR CONTRIBUTIONS.

T.I-K. and V.H. designed the research and experiments with input from S.K., S.C., S.F., S.M., A.K. and J.K.. T.I-K., C.L., M.B., K.B. and G.A. performed the research. T.I-K, C.L., M.B., K.B. and G.A. analyzed the data and S.C. analyzed the RNA-sequencing Data. T.I-K. and A.M. analyzed the CLIP data. R.M. performed

experiments for histology. The manuscript was written by T.I-K. and V.H. with critical input from S.F. and S.M..

COMPETING FINANCIAL INTERESTS.

The authors declare that they have no competing financial interests.

References

1. Acuto, O., Di Bartolo, V. & Michel, F. Tailoring T-cell receptor signals by proximal negative feedback mechanisms. *Nat Rev Immunol* **8**, 699-712 (2008).

2. Daley, S.R., Teh, C., Hu, D.Y., Strasser, A. & Gray, D.H.D. Cell death and thymic tolerance. *Immunol Rev* **277**, 9-20 (2017).

3. Zhan, Y., Carrington, E.M., Zhang, Y., Heinzel, S. & Lew, A.M. Life and Death of Activated T Cells: How Are They Different from Naïve T Cells? *Front Immunol* **8**, 1809 (2017).

4. Pasparakis, M. & Vandenabeele, P. Necroptosis and its role in inflammation. *Nature* **517**, 311-320 (2015).

5. Trebak, M. & Kinet, J.P. Calcium signalling in T cells. *Nat Rev Immunol* **19**, 154-169 (2019).

6. Feske, S. *et al.* A mutation in Orai1 causes immune deficiency by abrogating CRAC channel function. *Nature* **441**, 179-185 (2006).

7. Picard, C. *et al.* STIM1 mutation associated with a syndrome of immunodeficiency and autoimmunity. *N Engl J Med* **360**, 1971-1980 (2009).

8. Lacruz, R.S. & Feske, S. Diseases caused by mutations in ORAI1 and STIM1. *Ann N Y Acad Sci* **1356**, 45-79 (2015).

9. Feske, S., Skolnik, E.Y. & Prakriya, M. Ion channels and transporters in lymphocyte function and immunity. *Nat Rev Immunol* **12**, 532-547 (2012).

10. Hogan, P.G., Chen, L., Nardone, J. & Rao, A. Transcriptional regulation by calcium, calcineurin, and NFAT. *Genes Dev* **17**, 2205-2232 (2003).

11. Xiao, S. *et al.* FasL promoter activation by IL-2 through SP1 and NFAT but not Egr-2 and Egr-3. *Eur J Immunol* **29**, 3456-3465 (1999).

12. Rengarajan, J. *et al.* Sequential involvement of NFAT and Egr transcription factors in FasL regulation. *Immunity* **12**, 293-300 (2000).

13. Dzialo-Hatton, R., Milbrandt, J., Hockett, R.D., Jr. & Weaver, C.T. Differential expression of Fas ligand in Th1 and Th2 cells is regulated by early growth response gene and NF-AT family members. *J Immunol* **166**, 4534-4542 (2001).

14. La Rovere, R.M., Roest, G., Bultynck, G. & Parys, J.B. Intracellular Ca(2+) signaling and Ca(2+) microdomains in the control of cell survival, apoptosis and autophagy. *Cell Calcium* **60**, 74-87 (2016).

15. Kim, K.D. *et al.* ORAI1 deficiency impairs activated T cell death and enhances T cell survival. *J Immunol* **187**, 3620-3630 (2011).

16. Desvignes, L. *et al.* STIM1 controls T cell-mediated immune regulation and inflammation in chronic infection. *J Clin Invest* **125**, 2347-2362 (2015).

17. Zaccara, S., Ries, R.J. & Jaffrey, S.R. Reading, writing and erasing mRNA methylation. *Nat Rev Mol Cell Biol* **20**, 608-624 (2019).

18. Fu, Y., Dominissini, D., Rechavi, G. & He, C. Gene expression regulation mediated through reversible m□A RNA methylation. *Nat Rev Genet* **15**, 293-306 (2014).

19. Shulman, Z. & Stern-Ginossar, N. The RNA modification N(6)-methyladenosine as a novel regulator of the immune system. *Nat Immunol* (2020).

20. Gao, Y. *et al.* m(6)A Modification Prevents Formation of Endogenous Double-Stranded RNAs and Deleterious Innate Immune Responses during Hematopoietic Development. *Immunity* **52**, 1007-1021.e1008 (2020).

21. Li, H.B. *et al.* m(6)A mRNA methylation controls T cell homeostasis by targeting the IL-7/STAT5/SOCS pathways. *Nature* **548**, 338-342 (2017).

22. Tong, J. *et al.* m(6)A mRNA methylation sustains Treg suppressive functions. *Cell Res* **28**, 253-256 (2018).

23. Yao, Y. *et al.* METTL3-dependent m(6)A modification programs T follicular helper cell differentiation. *Nat Commun* **12**, 1333 (2021).

24. Grenov, A.C. *et al.* The germinal center reaction depends on RNA methylation and divergent functions of specific methyl readers. *J Exp Med* **218** (2021).

25. Sprent, J. & Surh, C.D. Writer's block: preventing m(6)A mRNA methylation promotes T cell naivety. *Immunol Cell Biol* **95**, 855-856 (2017).

26. Cao, G., Li, H.B., Yin, Z. & Flavell, R.A. Recent advances in dynamic m6A RNA modification. *Open Biol* **6**, 160003 (2016).

27. Zaccara, S. & Jaffrey, S.R. A Unified Model for the Function of YTHDF Proteins in Regulating m(6)A-Modified mRNA. *Cell* **181**, 1582-1595.e1518 (2020).

28. Lasman, L. *et al.* Context-dependent functional compensation between Ythdf m(6)A reader proteins. *Genes Dev* **34**, 1373-1391 (2020).

29. Liu, J. *et al.* A METTL3-METTL14 complex mediates mammalian nuclear RNA N6-adenosine methylation. *Nat Chem Biol* **10**, 93-95 (2014).

30. Wang, P., Doxtader, K.A. & Nam, Y. Structural Basis for Cooperative Function of Mettl3 and Mettl14 Methyltransferases. *Mol Cell* **63**, 306-317 (2016).

31. Schöller, E. *et al.* Interactions, localization, and phosphorylation of the m(6)A generating METTL3-METTL14-WTAP complex. *Rna* **24**, 499-512 (2018).

32. Knuckles, P. *et al.* Zc3h13/Flacc is required for adenosine methylation by bridging the mRNA-binding factor Rbm15/Spenito to the m(6)A machinery component Wtap/Fl(2)d. *Genes Dev* **32**, 415-429 (2018).

33. Yue, Y. *et al.* VIRMA mediates preferential m(6)A mRNA methylation in 3'UTR and near stop codon and associates with alternative polyadenylation. *Cell Discov* **4**, 10 (2018).

34. Bawankar, P. *et al.* Hakai is required for stabilization of core components of the m(6)A mRNA methylation machinery. *Nat Commun* **12**, 3778 (2021).

35. Ping, X.L. *et al.* Mammalian WTAP is a regulatory subunit of the RNA N6-methyladenosine methyltransferase. *Cell Res* **24**, 177-189 (2014).

36. Schwartz, S. *et al.* Perturbation of m6A writers reveals two distinct classes of mRNA methylation at internal and 5' sites. *Cell Rep* **8**, 284-296 (2014).

37. Lu, T.X. *et al.* A New Model of Spontaneous Colitis in Mice Induced by Deletion of an RNA m(6)A Methyltransferase Component METTL14 in T Cells. *Cell Mol Gastroenterol Hepatol* **10**, 747-761 (2020).

38. Borland, K. *et al.* Production and Application of Stable Isotope-Labeled Internal Standards for RNA Modification Analysis. *Genes (Basel)* **10** (2019).

39. Lee, P.P. *et al.* A critical role for Dnmt1 and DNA methylation in T cell development, function, and survival. *Immunity* **15**, 763-774 (2001).

40. Rubtsov, Y.P. *et al.* Regulatory T cell-derived interleukin-10 limits inflammation at environmental interfaces. *Immunity* **28**, 546-558 (2008).

41. Ohnmacht, C. *et al.* MUCOSAL IMMUNOLOGY. The microbiota regulates type 2 immunity through RORγt T cells. *Science* **349**, 989-993 (2015).

42. Hogquist, K.A. *et al.* T cell receptor antagonist peptides induce positive selection. *Cell* **76**, 17-27 (1994).

43. Barnden, M.J., Allison, J., Heath, W.R. & Carbone, F.R. Defective TCR expression in transgenic mice constructed using cDNA-based alpha- and beta-chain genes under the control of heterologous regulatory elements. *Immunol Cell Biol* **76**, 34-40 (1998).

44. Lin, Z. *et al.* Mettl3-/Mettl14-mediated mRNA N(6)-methyladenosine modulates murine spermatogenesis. *Cell Res* **27**, 1216-1230 (2017).

45. Sledzinska, A. *et al.* TGF-β signalling is required for CD4 T cell homeostasis but dispensable for regulatory T cell function. *PLoS Biol* **11**, e1001674 (2013).

46. Kieper, W.C. *et al.* Recent immune status determines the source of antigens that drive homeostatic T cell expansion. *J Immunol* **174**, 3158-3163 (2005).

47. Hoefig, K.P. *et al.* Defining the RBPome of primary T helper cells to elucidate higher-order Roquin-mediated mRNA regulation. *Nat Commun* **12**, 5208 (2021).

48. Körtel, N. *et al.* Deep and accurate detection of m6A RNA modifications using miCLIP2 and m6Aboost machine learning. *Nucleic Acids Res* (2021).

49. Buchbender, A. *et al.* Improved library preparation with the new iCLIP2 protocol. *Methods* **178**, 33-48 (2020).

50. Krakau, S., Richard, H. & Marsico, A. PureCLIP: capturing target-specific protein-RNA interaction footprints from single-nucleotide CLIP-seq data. *Genome Biol* **18**, 240 (2017).

51. Paris, J. *et al.* Targeting the RNA m(6)A Reader YTHDF2 Selectively Compromises Cancer Stem Cells in Acute Myeloid Leukemia. *Cell Stem Cell* **25**, 137-148.e136 (2019).

52. Zhu, Y. *et al.* The E3 ligase VHL promotes follicular helper T cell differentiation via glycolytic-epigenetic control. *J Exp Med* **216**, 1664-1681 (2019).

53. Little, N.A., Hastie, N.D. & Davies, R.C. Identification of WTAP, a novel Wilms' tumour 1-associating protein. *Hum Mol Genet* **9**, 2231-2239 (2000).

54. Vaeth, M., Kahlfuss, S. & Feske, S. CRAC Channels and Calcium Signaling in T Cell-Mediated Immunity. *Trends Immunol* **41**, 878-901 (2020).

55. Li, S. *et al.* The transcription factors Egr2 and Egr3 are essential for the control of inflammation and antigen-induced proliferation of B and T cells. *Immunity* **37**, 685-696 (2012).

56. Busch, A., Brüggemann, M., Ebersberger, S. & Zarnack, K. iCLIP data analysis: A complete pipeline from sequencing reads to RBP binding sites. *Methods* **178**, 49-62 (2020).

57. Bray, N.L., Pimentel, H., Melsted, P. & Pachter, L. Near-optimal probabilistic RNA-seq quantification. *Nat Biotechnol* **34**, 525-527 (2016).

58. Love, M.I., Huber, W. & Anders, S. Moderated estimation of fold change and dispersion for RNA-seq data with DESeq2. *Genome Biol* **15**, 550 (2014).

Figures

Figure 1

Wtap promotes the generation of gut RORγt+ regulatory T cells. a, b, Left panels, immunoblot analyses of Wtap (a) or Mettl3 (b) in MEF cells and Gapdh as a loading control. Data are representative of three biological replicates. Right panels, m6A abundance determined by LC/MS/MS analysis in the oligo-dT-purified mRNAs of Wtap or Mettl3-depleted and Cre expressing wildtype MEF cells. Data show three biological replicates. c, Incidence of mice showing symptoms of diarrhea and abdominal swelling. WT: n=9, KO: n=15. d, e, Body weight (d) and colon length (e) of 6 to 8-week old female mice are displayed. f, Representative image of colon from e. g, H&E stained colon tissue from Wtapfl/fl or Wtapfl/fl; Cd4-Cre mice. Scale bar, 10 μm. h, i, Flow cytometry of RORγt and Helios in CD4+Foxp3+ T cells in the lamina propria of the colon from Wtapfl/fl and Wtapfl/fl; Cd4-Cre mice (h) or Foxp3-Cre and Wtapfl/fl; Foxp3-Cre mice (i). The percentage of RORγt+Helios- Treg populations is shown on the right in h. Data presented

were derived from six mice (h) and four mice (i). j, IL-17a and IFNγ production in CD4+ T cells in lamina propria of the colon. Numbers in quadrants indicate percent cells in each. Percent of IL-17a and IFNγ positive cells is shown on the right.

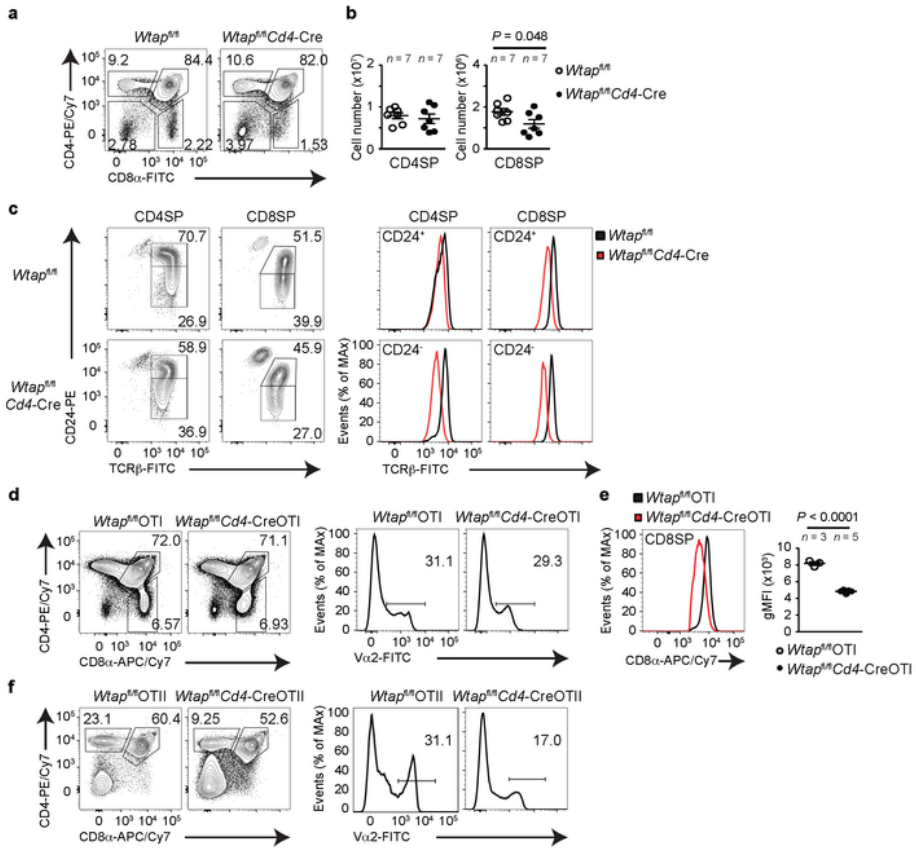

Figure 2

Figure 2

Wtap controls thymocyte development. a, b, Surface staining of thymocytes (a) and cellularity of CD4 SP or CD8 SP thymocytes (b) from Wtapfl/fl and Wtapfl/fl; Cd4-Cre mice. Data were derived from three

independent experiments. c, Surface staining of TCRβ and CD24 on gated CD4 SP or CD8 SP thymocytes. Numbers adjacent to outlined areas indicate percent cells in the CD24loTCRβhi or CD24hiTCRβlo gate. Histograms of TCRβ in the CD24lo or CD24hi gate are shown on the right. d, f Flow cytometry of thymocytes from Wtapfl/fl and Wtapfl/fl; Cd4-Cre mice expressing a transgene encoding the MHC class I-restricted OT-I TCR (d) or the MHC class II-restricted OT-II TCR (f). Left, staining of CD4 and CD8 of total thymocytes. Right, staining with antibody directed to the OT-I or OTII-specific variable region Vα2. Numbers above the bracketed lines indicate percent Vα2+ cells. Data are representative of two to three independent experiments. e. Histograms and geometric MFIs of CD8α in the CD8 SP gate are shown.

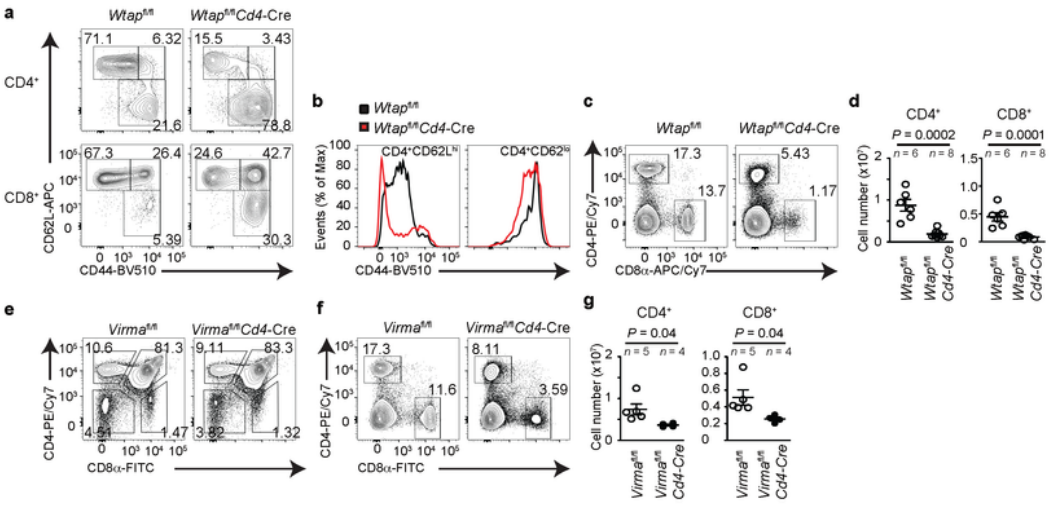

Figure 3

Figure 3

The m6A methyltransferase complex is required for T cell survival. a, Surface staining of CD44 and CD62L on CD4+ and CD8+ T cells in splenocytes from Wtapfl/fl and Wtapfl/fl; Cd4-Cre mice. Numbers adjacent to outlined areas indicate percent cells in each. Data are representative of three independent experiments. b, Histograms of CD44 in the CD62Llo or CD62Lhi gate are shown. Data are representative of three independent experiments. c-f, Surface staining of splenocytes (c, f) or thymocytes (e) and

cellularity of CD4+ or CD8+ T cells (d) from Wtapfl/fl and Wtapfl/fl; Cd4-Cre mice or Virmafl/fl and Virmafl/fl; Cd4-Cre mice. Numbers adjacent to outlined areas indicate percent cells in each in c, e and f. Presented data were derived from three independent experiments.

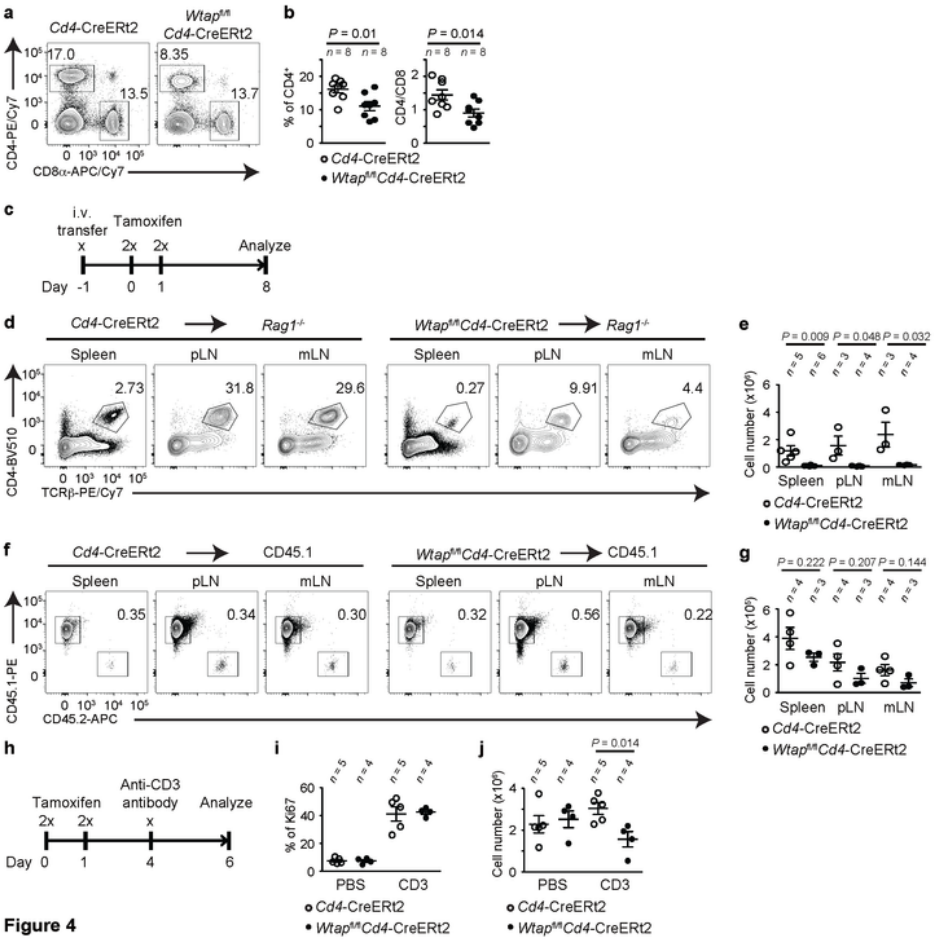

Figure 4

Figure 4

Wtap controls T cell survival upon TCR stimulation. a, Surface staining of splenocytes identifying CD4+ or CD8+ T cells from Cd4-CreERt2 and Wtapfl/fl; Cd4-CreERt2 mice that received tamoxifen gavage.

Numbers adjacent to outlined areas indicate percent cells in the respective gate. Data presented were derived from three independent experiments. b, Percentage of CD4+ T cells and ratio of CD4+ T cells to CD8+ T cells from a. c, Schematic representation of the adoptive transfer experiment. d, f, Flow cytometry of lymphoid organs from Rag1−/− (d) or CD45.1+ (f) mice 9 days after transfer of naive CD4+ T cells from Cd4-CreERt2 and Wtapfl/fl; Cd4-CreERt2 mice, assessed for expression of CD4 and TCRβ in d and CD45.1 and CD45.2 after gating on CD4+ population in f. Data presented were derived from two to three independent experiments. e, g, Cellularities of the transferred CD4+ T cells shown in d and f. h, Experimental scheme of the tamoxifen gavage of mice combined with anti-CD3 antibody injection. i, Analysis of the proliferating Ki67+ population within CD4+ T cells. j, Cellularity of CD4+ T cells from Cd4-CreERt2 and Wtapfl/fl; Cd4-CreERt2 mice that received tamoxifen gavage and anti-CD3 antibody injection. Data presented were derived from three independent experiments.

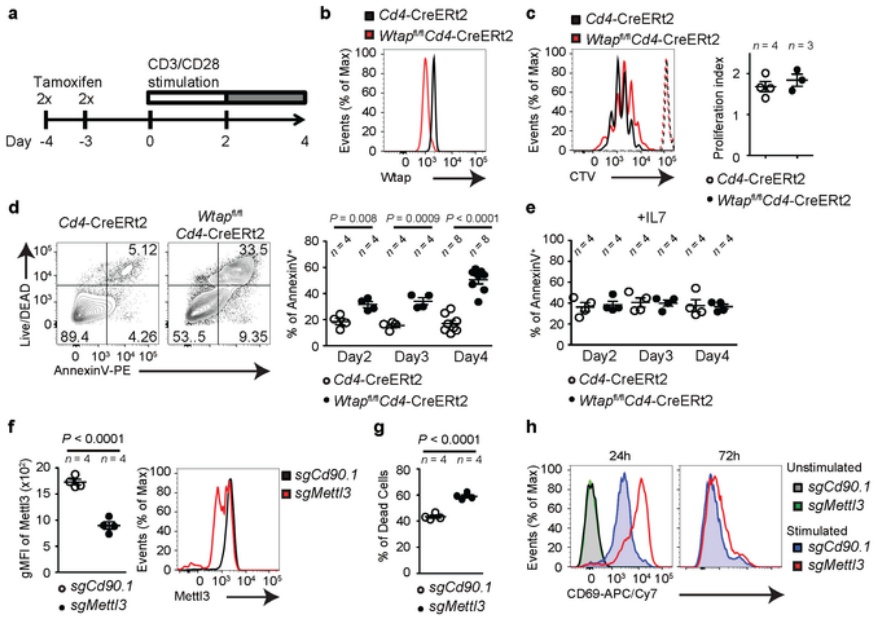

Figure 5

Figure 5

The m6A methyltransferase complex is essential for the survival of activated T cells. a, Schematic representation of the experiment involving oral gavage, followed by CD4+ T cell culture. b, Flow cytometry of CD4+ T cells from Cd4-CreERt2 and Wtapfl/fl; Cd4-CreERt2 mice using intracellular staining with anti-WTAP antibodies on day 0. Data are representative of three independent experiments. c, Flow cytometry analysis of CTV-labeled CD4+ T cells from Cd4-CreERt2 and Wtapfl/fl; Cd4-CreERt2 mice on day 4.

Unstimulated cells are shown as dotted lines. Data are representative of two independent experiments. The proliferation index is shown on the right. d, Flow cytometry of CD4+ T cells from Cd4-CreERt2 and Wtapfl/fl; Cd4-CreERt2 mice, stained with AnnexinV and LIVE/DEAD Fixable dye on day 4. Data are representative of three independent experiments. Percentage of AnnexinV+ population is shown in the right. e, Percentage of AnnexinV+ naive CD4+ T cells cultured in the presence of IL-7 on the indicated days. Data presented were derived from two independent experiments. f, g, Flow cytometry of CD4+ T cells transfected with sgRNA for Cd90 or Mettl3, stained with anti-METTL3 antibody on day 3 (f) and LIVE/DEAD Fixable dye on day 4 (g) after TCR re-stimulation. Data are representative of four biological replicate. h, Surface staining of CD69 in CD4+ T cells. Data are representative of four biological replicates.

Figure 6

Identification of m6A-modified transcripts. a, Gene ontology analysis of genes that were significantly upregulated or downregulated in 4'OH-tamoxifen induced Wtap deficient CD4+ T cells. The top-ranked terms are shown. Displayed categories were analyzed using the DAVID Bioinformatics Resource (version 6.8). b, Immunoblot analysis with a pan-Ythdf antibody in CD4+ T cells after stimulation with anti-CD3/anti-CD28 antibody (upper panel) or PMA and ionomycin (lower panel) using Gapdh as a loading control. Data are representative of three independent experiments. c, d, Pie chart of the distribution of the m6A-CLIP or Ythdf2-iCLIP peaks within introns, coding and untranslated regions. e, g, Venn diagram of overlaping peak regions in m6A-CLIP and Ythdf2-iCLIP experiments (e), or m6A-CLIP identified genes with DEGs from RNA-seq of Wtap deficient T cells (g). f, Volcano plot of m6A targets identified in g showing the -log10 p-value plotted against the log2 fold-change. h, Integrative Genomics Viewer (IGV) tracks displaying m6A-CLIP and Ythdf2-iCLIP read distribution. The read coverage is shown for merged replicates. Predicted DRACH motifs in the peak regions overlapping in the two CLIP experiments are marked with red arrowheads. i, The sequence of the DRACH motifs in the peak regions of Orai1 mRNA in h is shown.

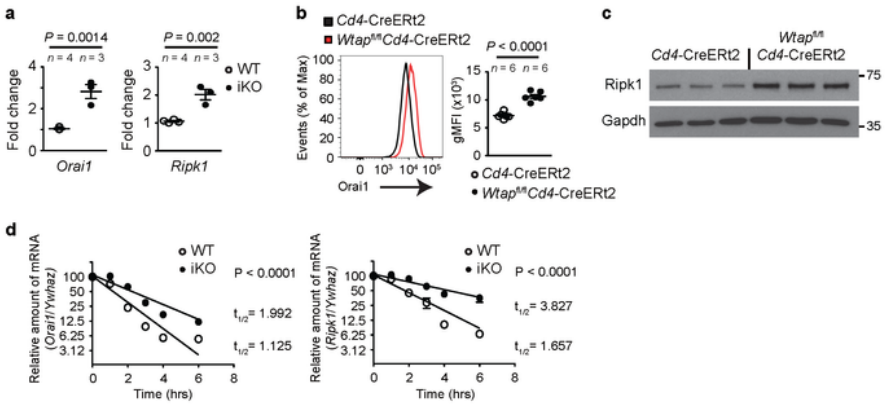

Figure 7

Figure 7

m6A methylation correlates with Orai1 and Ripk1 downregulation. a, qPCR analysis for Orai1 and Ripk1 for mRNA from iKO and control CD4+ T cells. Results are presented relative to Ywhaz expression. Data were derived from two independent experiments. b, Flow cytometry of CD4+ T cells from Cd4-CreERt2 and Wtapfl/fl; Cd4-CreERt2 mice that received tamoxifen gavage, cells were stained with anti-ORAI1 antibody on day 4 after stimulation. Data are representative of two independent experiments. Geometric MFI is

shown on the right. c, Immunoblot analysis of Ripk1 in CD4+ T cells from two different Cd4-CreERt2 or Wtapfl/fl; Cd4-CreERt2 mice that received tamoxifen gavage, followed by isolation and culture of CD4+ T cells. Gapdh serves as a loading control. Data shows three biological replicates.. d, Decay curves for Orai1 and Ripk1 mRNAs in iKO CD4+ T cells and control CD4+ T cells using Actinomycin D to terminate transcription of newly synthesized mRNAs. Data presented were derived from two independent experiments.

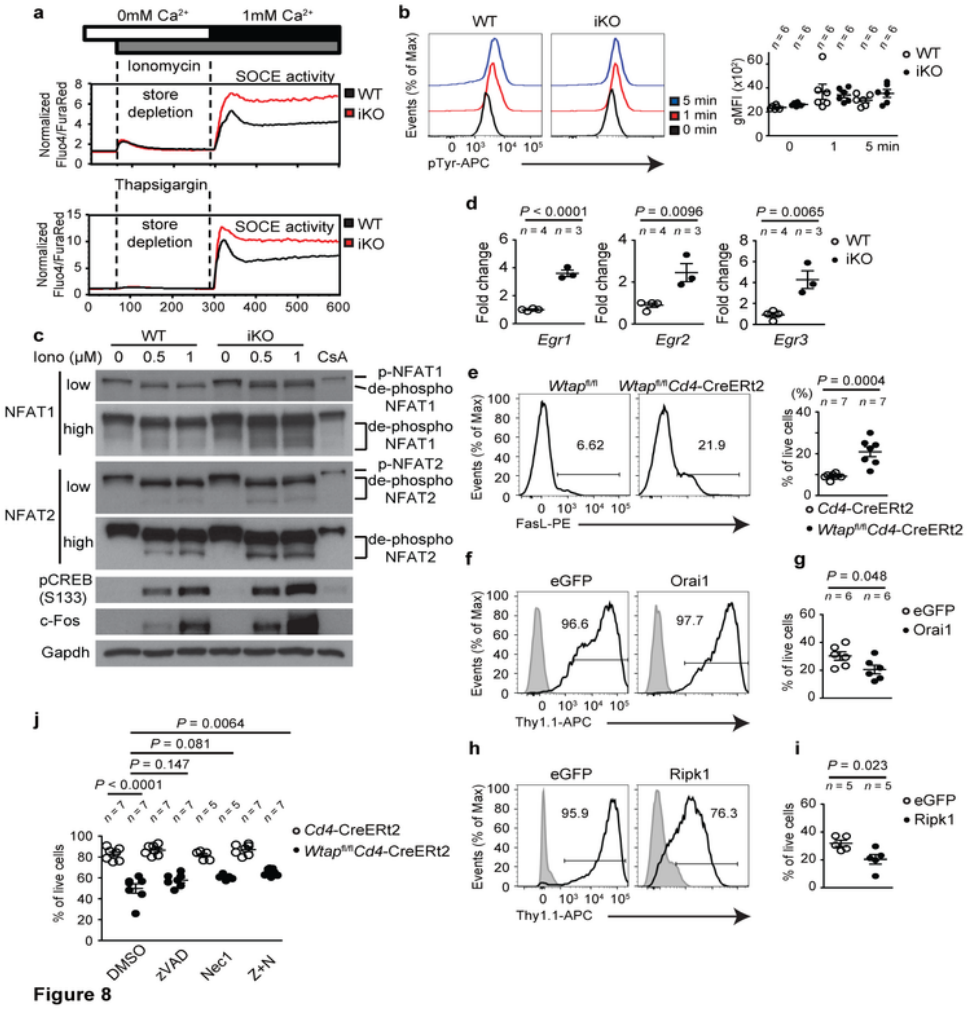

Figure 8

Figure 8

The m6A methyltransferase complex regulates TCR signaling. a, Analysis of Ca2+ store depletion and SOCE following ionomycin or thapsigargin stimulation in iKO and control CD4+ T cells. Data are representative of three independent experiments. b, Flow cytometry of iKO and control CD4+ T cells, assessed for expression of phospho-tyrosine after the re-stimulation with anti-CD3 and anti-CD28 antibodies. Data were derived from three independent experiments. c, Immunoblot analysis of NFAT1, NFAT2, pCREB and c-Fos in iKO and control CD4+ T cells that were stimulated with ionomycin or treated with cyclosporin A (CsA; 1 μM) for 20 min showing Gapdh as loading control. Data are representative of three independent experiments. d, qPCR analysis of iKO and control CD4+ T cells. Results are presented relative to Ywhaz expression. Data were derived from two independent experiments. e, Flow cytometry of CD4+ T cells from Cd4-CreERt2 and Wtapfl/fl; Cd4-CreERt2 mice that received tamoxifen gavage, cells were stained with anti-FasL antibody on day 4 after stimulation. Numbers above the brackets indicate percentage of cells in each gate, FasL+ percentages of CD4+ T cells from all experiments are shown on the right. Data represent three independent experiments. f-i, Flow cytometry of CD4+ T cells transduced with eGFP, Orai1 or Ripk1 encoding retroviruses, stained with anti-Thy1.1 antibody (f, h) and LIVE/DEAD Fixable dye (g, i) two days after TCR re-stimulation. Data are representative of three independent experiments. Grey histogram shows Thy1.1 negative cells. j, Flow cytometry of CD4+ T cells from Cd4-CreERt2 and Wtapfl/fl; Cd4-CreERt2 mice that received tamoxifen gavage. Naive CD4+ T cells were cultured in the presence of zVAD-fmk (40 μM) and/or Nec1 (10 μM). AnnexinV and the LIVE/DEAD Fixable dye were used for staining of cells on day4. Data are representative of three independent experiments.

Supplementary Files

This is a list of supplementary files associated with this preprint. Click to download.

- ExtendedDataFigure1.pdf
- ExtendedDataFigure2.pdf
- ExtendedDataFigure3.pdf
- ExtendedDataFigure4.pdf
- ExtendedDataFigure5.pdf
- ExtendedDataFigure6.pdf
- ExtendedDataFigure7.pdf
- ExtendedDataFigure8.pdf
- ExtendedDataFigureLegends.docx
- SupplementaryTable1.xlsx